

1 *Manuscript Draft*

2 **The Guaymas Basin Subseafloor Sedimentary Archaeome Reflects Complex**
3 **Environmental Histories**

4
5 Gustavo A. Ramírez^{1,2*}, Luke J. McKay^{3,4}, Matthew W. Fields^{4,5}, Andrew Buckley¹, Carlos
6 Mortera⁶, Christian Hensen⁷, Ana Christina Ravelo⁸ & Andreas P. Teske¹

7
8 Author affiliations:

9 1: Department of Marine Sciences, University of North Carolina at Chapel Hill, NC, USA.

10 2: College of Veterinary Medicine, Western University of Health Sciences, Pomona, CA, USA.

11 3: Department of Land Resources and Environmental Sciences, Montana State University, Bozeman,
12 MT, USA.

13 4: Center for Biofilm Engineering, Montana State University, Bozeman, MT, USA.

14 5: Department of Microbiology and Immunology, Montana State University, Bozeman, MT, USA.

15 6: Instituto de Geofísica, Universidad Nacional Autónoma de México, Coyoacán, México.

16 7: GEOMAR Helmholtz Centre for Ocean Research, Kiel, Germany.

17 8: Ocean Sciences Department, University of California, Santa Cruz, CA, USA.

18
19
20
21
22
23
24 *: Corresponding author

25
26 Correspondence:

27 Gustavo A. Ramírez

28 gara1985@email.unc.edu

29 gramirez@westernu.edu

30 zombiephylotype@gmail.com

31

32

33 **Abstract**

34 We explore archaeal distribution and environmental niche differentiation in sedimentary
35 subseafloor habitats of Guaymas Basin and the adjacent Sonora Margin, located in the Gulf of
36 California, México. Specifically, we survey diverse subseafloor habitats on the Guaymas Basin
37 flanking regions that are extending from the spreading center, termed here “off-axis” sites.
38 Sampling locations include (i) control sediments without hydrothermal or seep influence, (ii)
39 Sonora Margin sediments underlying oxygen minimum zone water, (iii) compacted, highly
40 reduced sediments from a pressure ridge with numerous seeps at the base of the Sonora Margin,
41 and (iv) sediments impacted by hydrothermal circulation at the off-axis Ringvent site.
42 Generally, archaeal 16S rRNA gene datasets are largely comprised of Bathyarchaeal lineages,
43 members of the Hadesarchaea, MBG-D, TMEG, and ANME-1 groups. The most frequently
44 observed 25 OTUs belong to members of these lineages, and correspond to approx. 40 to 80%
45 of the sequence dataset in each sediment sample. Differential distribution patterns of these
46 archaeal groups in downcore sediments uniquely characterize each major sedimentary
47 environment. Variations in archaeal community composition reflect locally specific
48 environmental challenges throughout the greater Guaymas Basin area. Background sediments
49 are divided into surface and subsurface niches, reflecting increased selection of the archaeal
50 community downcore. In sum, the environmental setting and history of a particular site, not
51 isolated biogeochemical properties out of context, control the subseafloor archaeal
52 communities in Guaymas Basin and Sonora Margin sediments.

53

54 **Introduction**

55 Guaymas Basin, located in the Gulf of California, México, is a young marginal rift basin where
56 active seafloor spreading generates northeast-to-southwest trending axial troughs surrounded
57 on both sides by extensive flanking regions (Lizarralde et al., 2007). In contrast to mid-ocean
58 spreading centers, axial troughs and flanking regions of Guaymas Basin are covered by thick,
59 organic-rich sediments that represent a combination of terrigenous input and biogenic
60 sedimentation from the highly productive water column (Calvert, 1966). Magmatic intrusions,
61 or sills, are embedded within the thick sediment layers, where they drive hydrothermal
62 circulation (Lonsdale and Becker, 1985) and thermally alter buried organic matter (Seewald et
63 al., 1990), in the process generating complex petroleum compounds (Didyk and Simoneit,
64 1989), light hydrocarbons and methane (Welhan and Lupton, 1987), carboxylic acids (Martens,
65 1990), and ammonia (Von Damm et al., 1985). Since the sediments act as a heat-retaining
66 thermal blanket, magmatic activity and organic matter alteration and mobilization are not
67 limited to the spreading center but also occur at considerable distance, up to 50 km off-axis
68 (Lizarralde et al., 2010). Many of these off-axis sites resemble cold seeps, where methane
69 advection is linked to pathways formed by deeply buried magmatic sills (Geilert et al., 2018).
70 If the underlying sill is sufficiently shallow and hot, the hydrothermal underpinnings of these
71 off-axis sites becomes visible; the recently described Ringvent site provides an example (Teske
72 et al., 2019).

73 In contrast, the Sonora Margin harbors classical cold seeps where sediment compaction
74 drives reducing, methane-rich seep fluids to the surface. Numerous seep sites with carbonate
75 outcrops and cold seep fauna have been observed on an eroding pressure ridge that follows the
76 transform fault at the base of the Sonora Margin (Simoneit et al., 1990; Paull et al., 2007); the
77 seep communities at these sites are largely based on methanotrophy and sulfide oxidation
78 (Portail et al., 2015). Seep communities and sulfide-oxidizing microbial mats are also
79 widespread on the Sonora Margin slopes (Vigneron et al., 2014; Cruaud et al., 2017).

80 Finally, most of the extensive flanking regions of Guaymas Basin and the Sonora
81 Margin slope are covered by sediments without particular seep or hydrothermal influence;
82 these sediments consist of mixed terrigenous runoff and biogenic components, dominated by
83 diatoms (Calvert, 1966). Sediments on the upper Sonora Margin underlying the oxygen
84 minimum at ca. 600 to 800 m depth, lack bioturbation and show finely laminated, seasonally
85 changing sedimentation patterns of spring diatom blooms and terrestrial runoff during late
86 summer rains (Calvert, 1964).

87 Here, we survey the distribution of archaea in diverse sedimentary environments
88 located in the greater Northern Guaymas Basin and Sonora Margin regions. Sampling areas
89 include background sediments from the Guaymas Basin flanking regions, Sonora Margin
90 sediment within the oxygen minimum zone, reducing sediment with cold seep characteristics
91 from the base of the Sonora Margin, and sediment from the off-axis Ringvent site where
92 hydrothermal circulation and methane seepage is driven by a gradually cooling, buried shallow
93 sill. We expand a previous limited sequencing survey of these sediments focused on just one
94 of these sites (Teske et al., 2019) by: i) extending the geochemical analyses, ii) increasing the
95 sampling resolution used for molecular sequencing (from one or two samples per site to ~1-
96 meter intervals for all sites), iii) providing a wide breadth of comparative ecological analyses,
97 and iv) discussing the potential implications of our results at a basin-wide scale.

98

99 **Results**

100 *1. Sediment and porewater geochemistry*

101 We surveyed archaeal distribution at six sites on the northwestern and southeastern off-axis
102 regions of Guaymas Basin and on the Upper Sonora Margin (Figure 1, Table S1). These
103 locations represent four different environmental settings: (i) Sediments on the Guaymas Basin
104 flanking regions without hydrothermal or seep activity, represented by cores Cont03, Cont10
105 and Cont13; (ii) the oxygen minimum zone on the upper Sonora Margin (Calvert, 1964),
106 represented by core OMZP12, (iii) compacted, highly reducing seep sediments from a pressure
107 ridge, running along the transform fault that is cutting across the base of the Sonora Margin
108 (Simoneit et al. 1990, Paull et al. 2007), represented by core Seep06, and (iv) the Ringvent site,
109 characterized by off-axis hydrothermal circulation (Teske et al., 2019), represented by core
110 RNVP11 (Figure 1). At each site, sediment piston cores ranging from 5 to 486 cm below the
111 seafloor (cmbsf) were collected and geochemically characterized (Figure 2). The sediments are
112 geologically young, ranging in age between ~0.05K and ~20K calendar years, as determined
113 by C14 dating (Teske et al., 2019). The different cores show distinct geochemical
114 characteristics.

115 Core SeepP06 contains sulfide in millimolar concentrations throughout the core.
116 Below the zone of sulfate-dependent methane oxidation at 1 m depth, methane accumulated to
117 the highest concentrations of this survey, > 10 mM. Porewater DIC concentrations were
118 consistently high and increased from 15 mM near the interface to nearly 50 mM with depth.
119 These methane and DIC concentrations reached and in part exceeded the highest concentrations
120 previously measured in Sonora Margin seep fluids (Paull et al., 2007). Sediments of core

121 SeepP06 yielded only approximately half of the porewater volumes of other cores, indicating
122 porewater loss by pressure-induced compaction. Thus, core SeepP06 represents sulfidic,
123 methane- and DIC-soaked, compacted seep sediments from the pressure ridge aligned with the
124 transform fault at the lower Sonora Margin (Simoneit et al., 1990; Paull et al., 2007).

125 Cores Cont03 and ContP10 share similar methane, sulfate, sulfide, and DIC profiles
126 indicative of non-reducing conditions where sulfate-reducing and methanogenic activities
127 remain minimal and biogenic sulfide and methane occur only in micromolar trace
128 concentrations. With TOC between 4 and 6 wt %, the sediments of core ContP10 are organic
129 rich and represent the hemipelagic seafloor sediments of Guaymas Basin that receive ample
130 biogenic sedimentation, mostly by diatoms (Calvert, 1966). The $\delta^{13}\text{C}$ values ranging from -
131 20.12 to -20.51‰ are consistent with sedimentary organic material resulting predominantly
132 from phytoplankton input (Teske et al., 2002). Slowly increasing $\delta^{15}\text{N}$ values ranging from
133 9.04 to 10.17‰, and gradually increasing C:N ratios downcore are consistent with microbial
134 utilization of nitrogen compounds in sedimentary biomass.

135 Contrasting with nearby core Cont10, Core RNVP11 shows the biogeochemical
136 signatures of seawater inmixing and previous hydrothermal alteration at Ringvent (Teske et al.,
137 2019). Subsurface-derived porewater methane in high concentrations of 1 to 1.5 mM coexists
138 with porewater sulfate near seawater levels; sulfide is largely absent and reaches 10 to 100 μM
139 only below 3 m depth. Core RNVP11 also stands out by having the lowest DIC concentrations
140 of all cores, approaching seawater DIC in the upper layers. Below 1 mbsf, organic carbon $\delta^{13}\text{C}$
141 values are the lowest for all cores, whereas C/N ratios are the highest, suggesting the influence
142 of isotopically light and nitrogen-depleted fossil carbon sources (Figure 2). In contrast to other
143 cores, Core RNVP11 shows a strong gradient of dissolved silica, increasing from 0.5 to 0.6
144 mM at the surface (similar to ContP10) towards 0.9 to 1 mM at the bottom (Figure 2 I). Silica
145 dissolution is considered a marker of hydrothermal activity (Peter and Scott, 1988), and leads
146 to elevated concentrations of dissolved silica in the water column of Guaymas Basin (Campbell
147 and Gieskes, 1984).

148 Core OMZP12 differs from all other cores by its location in the oxygen minimum zone
149 on the Sonora Margin slope (Calvert, 1964). Bottom water anoxia allows millimolar
150 concentrations of porewater sulfide to permeate the entire sediment core including the surface,
151 otherwise only seen in core SeepP06. The sulfate-methane transition zone occurs at
152 approximately 1 and 2m depth for SeepP06 and OMZP12, respectively. Similar to core
153 SeepP06, porewater DIC increases rapidly with depth, with a maximum value of 33mM at 254

154 cmbsf. Sediment TOC, $\delta^{13}\text{C}$, $\delta^{15}\text{N}$, and C:N ratio values generally resemble those of other cores
155 in this survey.

156 Core ContP13, collected on the southeastern flanking region, differs from other cores
157 by terrestrial input from the Yaqui River. Methane, sulfate, sulfide and DIC concentrations for
158 this core follow similar depth profiles as observed for cores ContP03 and ContP10. However,
159 TOC varies between ~1 and ~5 wt % in the first meter of sediment and between ~3 and ~6 wt
160 % below, suggesting sedimentation pulses of varying organic carbon load. Sediment organic
161 matter $\delta^{13}\text{C}$, $\delta^{15}\text{N}$ and C:N ratios fall within the range of values observed for other cores in this
162 survey.

163

164 2. Diversity of the Guaymas Basin archaeome

165 Rarefaction curves are plotted separately for samples in approx. 1 meter depth intervals
166 to examine potential downcore trends (Figure 3). Starting at 3 m depth, observed species
167 richness based on rarefaction summaries are lower in Ringvent (Core RNVP11) sediment
168 compared to other sediments (Figure 3, Table S2). Substantially more sequence reads, and thus
169 a higher number of observed species, were recovered from the Sonora Margin OMZ sediment
170 (Core OMZP12) relative to the other surveyed sites, below 1 m depth (Figure 3 C-E). To
171 account for different sequencing depths without resorting to rarefying the dataset (McMurdie
172 and Holmes, 2014), we estimated total diversity using a non-linear regression model for ratios
173 of consecutive frequency counts, a state-of-the-art method addressing the issue of heterologous
174 sequencing depths affecting richness estimates (Willis and Bunge, 2015). Results from this
175 model indicate no statistically significant ($P_{\text{val}} < 0.05$) differences amongst surveyed sites
176 (Figure S1).

177 When beta diversity of the archaeal communities was examined for correlations with
178 environmental metadata using two-dimensional principal coordinate analysis, distinct
179 clustering patterns are observed (Figure 4A). Surface communities for all cores except
180 OMZP12 tightly cluster along negative axis 1 values. All OMZP12 samples cluster along axis
181 1 values greater than 0.01 independently of sediment depth. Separation along axis 2 partitions
182 the SeepP6, RNVP11, and OMZP12 cores (with positive axis 2 values), from subsurface
183 samples of control cores ContP3, ContP10, and ContP13 with negative axis 2 values; the
184 surface samples of these cores cluster separately (Figure 4A). The influence of environmental
185 factors (*i.e.*: methane, sulfate, sulfide, DIC, water depth, and sediment depth) on community
186 ordination is complex (Figure 4B-G), and it appears likely that clustering patterns are not

187 driven by these environmental parameters alone. Water column depth (Figure 4F) appears to
188 drive core OMZP12 clustering along larger positive values for axis 1, but most likely represents
189 a proxy for the influence of the oxygen minimum zone at this depth.

190

191 *3. Network analysis*

192 Network analysis based on the co-occurrence of all OTUs in each sample reveals that the
193 deepest communities recovered from Core RNVP11 exhibit the greatest degree of separation
194 (Figure 5). At a maximum ecological (Bray-Curtis) distance of 0.8 (*i.e.*: the maximum distance
195 allowed between two samples to be considered connected in the graphical model), most
196 samples share taxa co-occurrence patterns, except for the deepest communities from core
197 RNVP11 (Figure 5A). Decreasing the minimum ecological distance in the model to 0.5,
198 resolves three independent network clusters (Figure 5B). Here, the two deepest samples from
199 core RNVP11 share similar taxa co-occurrence patterns only with each other and are excluded
200 from the two emergent additional networks. In one of these networks, communities near the
201 seawater interface of all cores, with the exception of core RNVP11, connect at no more than
202 1-degree of separation. Interface sample SeepP06 5cmbsf connects the near-interface sample
203 cluster to all core SeepP6 seafloor (depth > 1mbsf) samples. A third independent network
204 shows non-random taxa co-occurrence amongst seafloor control sediments (cores ContP3,
205 ContP10, ContP13), a seafloor and a near-interface sample from core RNVP11, and all
206 samples from core OMZP12; the three deepest OMZP12 samples are only peripherally
207 connected (Figure 5B).

208

209 *4. Community composition*

210 Class-level community descriptions (SILVA132) assigned large membership fractions of the
211 archaeal communities to the Bathyarchaeia, Hadesarchaeaeota, and Thermoplasmata (Figure
212 6). The Class Methanomicrobia, comprising methane-producing and methane-oxidizing
213 members of the Euryarchaeota, was detected in multiple cores, but appeared most frequently
214 at depth in core SeepP06. An in-depth summary of the Methanomicrobia reveals the presence
215 of methanogenic families (eg: Methanomicrobiaceae) and anaerobic, methane-oxidizing
216 ANME lineages (ANME-1, various ANME-2). Notably, ANME-1 archaea dominate core
217 SeepP06 sequence assignments comprising nearly 40% of the total community at 394 cmbsf
218 in this core (Figure S2, Table S3). Order- or higher-level community taxonomic descriptions
219 for all samples generally contained 60% or greater unclassified community fractions (data not
220 shown) when automated taxonomic assignments were performed. In order to not rely on the

221 uncertain output of taxonomy pipelines, and to resolve archaeal taxonomy assignments in a
222 manner that is consistent with broadly accepted usage (Spang et al., 2017), we also describe
223 community composition based on phylogenetic placement of dominant sequence variants for
224 the most numerous 25 Operational Taxonomic Units (OTUs).

225 The majority of high-quality sequences in this study (73.0%) clustered into 25 OTU
226 lineages (Figure 7A). Archaeal communities were largely dominated by OTU lineages related
227 to the Bathyarchaea (16 out of the top 25 OTUs). OTUs 01 to 03, the three most abundant
228 lineages, belong to the MCG-1, MCG-2, and MCG-3 Bathyarchaea subgroups (Kubo et al.,
229 2012) respectively, with close relatives recovered from Guaymas Basin and globally-dispersed
230 seafloor habitats (Figure 7B). High abundance lineages related to the Marine Benthic
231 Group-D within the Thermoplasmata (MBG-D; OTUs 04, 10, 11, 21, and 23) and the
232 Terrestrial Miscellaneous Euryarchaea Group (TMEG; OTU 08) were recovered from all cores
233 and core depths except the subsurface of Ringvent (Core RNVP11, depth > 1mbsf). Two highly
234 abundant lineages represented by OTUs 05 and 18 (Figure 7C) were recovered from every core
235 except core SeepP06, and identified as relatives of the Hadesarchaea, formerly known as South
236 African Gold Mine Euryarchaea Group (SAGMEG)-1 (Baker et al., 2016). Lastly, OTU 14
237 clustered within anaerobic ANME-1 methanotrophs and was most closely related to ANME-1
238 phylotypes from cold seep, hydrate and brine habitats; OTU 14 did not affiliate with the
239 thermophilic ANME-1 Guaymas lineage recovered from hydrothermally active, hot sediments
240 in Guaymas Basin (Biddle et al., 2012) (Figure 7C).

241

242 *5. Differential taxon abundance estimations across ecological niches*

243 Differential abundance analyses (Wald Test, Pval = 0.01) were performed on various
244 ecological-models following potential environmental niches suggested by ordination patterns
245 (Figure 8). Only OTU lineages amongst comparison groups containing more than 100
246 sequences were used for each test. We tested the influence of sediment depth in the absence of
247 seepage or hydrothermal influence, the impact of the oxygen minimum zone waters on surficial
248 and subsurface sediments, and the effect of hydrothermal disturbance. These analyses have to
249 be qualified by the fact that they are based on patterns of sequence frequencies, which are
250 derived from the archaeal community but do not necessarily represent it in identical
251 proportions.

252 To test the estimated differential abundance of archaeal community members in near-
253 surface (depth < 1mbsf) and subsurface (depth > 1mbsf) communities under conditions of
254 normal hemipelagic sedimentation, we selected cores ContP3, ContP10, and ContP13; these

255 cores lack hydrothermal, seepage or OMZ influence and, therefore, show the archaeal
256 community of organic-rich Guaymas Basin sediments in the absence of these selective factors.
257 Here, over 43% of OTUs ($n > 100$ seqs) are differentially enriched with depth (Figure 8A &
258 B). Most differentially abundant taxa are estimated to be significantly less abundant in near-
259 surface relative to subsurface control sediment (Figure 8B). Subsurface enriched lineages
260 include members of various Bathyarchaeal groups (MCG-1, MCG-3, and MCG-6), a TMEG
261 lineage (OTU 08) closely related to clones previously recovered from Guaymas Basin, and a
262 Hadesarchaea lineage (OTU 18) whose closest relatives are clones from deep Mediterranean
263 waters (Figures 7B & C). Among the top 25 OTUs in this study, the only highly abundant
264 lineage that is significantly ($P_{val} = 0.01$) enriched in near-surface relative to subsurface control
265 sediment (Figure 8A), is OTU 07, related to Guaymas Basin and Indian estuary sediment
266 MCG-6 clones (Figure 7B). The same lineage was also found to occur preferentially in surficial
267 estuarine sediments in the White Oak River, while avoiding the sulfide-rich, sulfate-reducing
268 and methanogenic conditions just a few centimeters downcore (Lazar et al., 2015).

269 When archaeal abundance in all oxygen minimum core OMZP12 samples was checked
270 against the shallow sediment samples of the control cores (ContP03, ContP10, ContP13, see
271 Figure 8C and D), over 50% of archaeal OTUs ($n > 100$ seqs) present in surficial controls were
272 differentially enriched in core OMZP12. Of the 25 most highly abundant OTUs in this study,
273 those that were differentially abundant in this comparison (14 OTUs) were predominantly
274 enriched in core OMZP12 (eleven of fourteen high abundance OTUs, Figure 8D). Only OTUs
275 07, 09, and 21, representing the Bathyarchaeal groups MGC-6 and MCG-2, and a MBG-D
276 lineage, respectively, were enriched in surficial control sediment (Figure 8D).

277 We also tested for differentially abundant taxa between all core OMZP12 samples and
278 subsurface control sediment (Figure 8E). Here, only 31.1% of OTUs ($n > 100$ seqs) were
279 differentially enriched; of the 25 most abundant OTUs in this study only 4 were differentially
280 enriched. Of these four differentially enriched archaeal OTUs, OTUs 15 and 20, Bathyarchaeal
281 lineages in the MCG-1 and MCG-2, respectively, were enriched in subsurface control
282 sediment. OTU 06 within the MCG-2 group, and OTU 19, an MCG lineage tenuously related
283 (bootstrap value $< 70\%$) to MCG-6, were enriched in core OMZP12. Overall, archaeal types
284 occurring in anoxic subsurface sediments of core OMZP12 resemble those in other subsurface
285 cores to a large extent.

286 The hydrothermally influenced Ringvent core RNVP11 was compared against control
287 core ContP10, located only 1.6 km further west, at the same depth and local sedimentation
288 regime (Figure 8F-H). In surficial sediment (> 1 mbsf) this comparison revealed only one

289 differentially enriched phylotype, OTU 18 within the Hadesarchaea (Figure 8G). On the other
290 hand, the comparison of subsurface (>1 mbsf) communities identified 43 OTUs, or 61% of all
291 shared OTUs ($n > 100$ seqs), as differentially abundant between these two sites (Figure 8H).
292 Focusing on the top 25 highest abundance OTUs in this study, eleven OTUs were differentially
293 enriched. Eight taxa, comprised of Bathyarchaeal, TMEG, MBG-D, and ANME-1
294 representatives, were significantly enriched in subsurface control sediment relative to Ringvent
295 subsurface sediment (OTUs: 07, 08, 10, 11, 14, 15, 16, and 23). The remaining three taxa
296 (OTUs 06, 12, and 25), enriched in the Ringvent subsurface, were classified as Bathyarchaea
297 related to the MCG-1 and MCG-2 subgroups.

298 Core SeepP06, from compacted seep sediments, was checked against both shallow and
299 subsurface sediment samples of the control cores (ContP03, ContP10, ContP13, Figure 7I-K).
300 41% of archaeal OTUs ($n > 100$ seqs) present in shallow controls and seep sediment were
301 differentially enriched (Figure 8J). Of the 25 most highly abundant OTUs, most were
302 predominantly enriched in seep sediment and included lineages classified as ANME-1, MBG-
303 D, and TMEG (Figure 8J). When comparing differentially abundant taxa between core
304 SeepP06 and subsurface control sediment, almost 53% of archaeal OTUs ($n > 100$ seqs) were
305 differentially enriched (Figure 8K). Most of the OTUs in this comparison, including the most
306 abundant OTUs in this study (OTUs 01-03), were enriched in control subseafloor sediments
307 rather than in core SeepP06 sediment (Figure 8K).

308

309 **Discussion**

310 *1. Complex determinants of archaeal ecosystem structure*

311 Overall, complex physical and geochemical factors structure sedimentary habitats and depth-
312 related niches for archaea in Guaymas Basin. Archaeal community ordination patterns reveal
313 niche differentiation and some unexpected clustering patterns among the different sites (Figure
314 4A).

315 Most notably, surficial communities of background control sediments ContP03,
316 ContP10, and ContP13, at 5 to 10 cm depth, cluster away from their respective subsurface
317 communities near 1 m depth and below (Figure 4A), implying an ecological bifurcation into
318 two distinct niches. Taxa co-occurrence network patterns support this differentiation between
319 shallow and subseafloor control sediment sites (Figure 5B). Possibly, the availability of
320 electron acceptors such as oxygen, nitrate or oxidized metals drives the depth-dependent niche
321 separation observed in background control sediment sites (ContP03, ContP10, and ContP13).
322 Surface archaeal communities continually change as sediment layers accumulate; given high

323 sedimentation rates of 0.23 to 1 mm/y at Guaymas Basin (Teske et al., 2019), it takes approx.
324 1000 to 4000 years for background surface communities to transition to subsurface
325 communities at 1 m depth. Interestingly, shallow vs subsurface differentiation is less apparent
326 in seep, OMZ or hydrothermally influenced sites (Figure 5B); parameters other than sediment
327 depth or surficial redox regime are shaping archaeal community composition in seepage- or
328 hydrothermally-influenced habitats, compared to the control sites.

329 The cores SeepP06 and RNVP11 represent different geochemical regimes
330 (compaction-induced continental margin seepage vs hydrothermal circulation, respectively),
331 yet these two sites cluster tightly in ordination space (Figure 4). Individual geochemical factors,
332 for example, the sulfidic, methane- and DIC-rich conditions in SeepP06 would have indicated
333 that OMZP12 should be its closest equivalent (Figure 2). The unexpected clustering of SeepP06
334 and RNVP11 suggests that factors beyond current geochemical conditions, for example recent
335 environmental disturbance, can influence archaeal community structure. At Ringvent
336 (RNVP11), sedimentary community diversity may have been reduced during prior episodes of
337 thermal purging or high methane flux (Teske et al., 2019), selecting for a resilient, yet
338 potentially less diverse (Figure 3), “survivor” community.

339 Lastly, community ordination differentiates OMZ sediment from all other sedimentary
340 habitats (Figure 4). While water depth appears to have a strong influence on OMZ sediment
341 ordination (Figure 4F), we propose that differences in redox potential at the sediment interface
342 due to its direct contact with oxygen-depleted water (Calvert, 1964) rather than water column
343 depth, is the key environmental constraint driving the ordination patterns of OMZ sediment.

344

345 2. A “forest view” of Archaea in Guaymas Basin sediments

346 Archaea observed in this sedimentary habitat survey belong to the Bathyarchaea, the MBG-D
347 and TMEG lineages within the Thermoplasmatales, the Hadesarchaea (SAGMEG), and
348 ANME-1 lineages, as shown previously in a sequencing survey using different archaeal
349 primers (Teske et al. 2019). The uncultured Bathyarchaea and MBG-D archaea pronouncedly
350 dominate the dataset, and cold anoxic marine sediments globally (Kubo et al., 2012; Lloyd et
351 al., 2013). Bathyarchaea play an important role, tantamount to that of the domain Bacteria, in
352 the remineralization of complex organic matter in marine sediment (Lloyd et al., 2013); some
353 of their members (MCG-8 lineage) use lignin, the second most common biopolymer on Earth,
354 as an energy source (Yu et al., 2018). Since Bathyarchaeota harbor the Woods-Ljungdahl
355 pathway, they are implied in acetogenic subsurface metabolism (He et al., 2016), but it remains
356 open whether acetogenic pathways are used for net autotrophy, or derive their substrates from

357 organic carbon sources (Lever et al., 2010); similar considerations apply to the metabolically
358 versatile MBG-D archaea (Zhou et al., 2019). Some Bathyarchaea harbor genes of the MCR
359 complex, suggesting methylotrophic methanogenic activity and, perhaps, syntrophic
360 interactions with sulfate reducing bacteria leading to the anaerobic oxidation of methane
361 (Evans et al., 2015). However, the dominant Bathyarchaea OTUs recovered in this study
362 (MCGs 1, 2, 3, 6, and 13, Figure 7B) are only distant relatives of methane-cycling marine
363 Bathyarchaea, which fall into MCGs 15 and 16 (Evans et al., 2015). Hadesarchaea, originally
364 described as the South-African Gold Mine Miscellaneous Euryarchaeal Group (SAGMEG),
365 are metabolically versatile anaerobic heterotrophs with the metabolic potential for CO and H₂
366 oxidation coupled with nitrite reduction to ammonia and are found in environments across
367 broad (4 to 80°C) thermal ranges (Baker et al., 2016). One of two frequently recovered
368 Hadesarchaea lineages (OTU 05) is conspicuously enriched in subsurface sediment in Ringvent
369 (RNVP11), where low observed sequence richness (Figure 3) coincides with evidence (high
370 silica porewater concentrations at depth indicative of a thermal dissolution of sedimentary
371 diatoms, Figure 2I) for a thermal purge in the past (Teske et al., 2019).

372 Unsurprisingly, the methane-cycling Methanomicrobia are rare in background
373 sediments (ContP03, Cont10, and Cont13) but are strongly enriched in core SeepP6 and, to a
374 much lower extent (slightly over 2%), in core OMZP12 at 204 cm depth (Figures 6 and S2).
375 Interestingly, a single ANME-1 OTU lineage, OTU14, is highly enriched in SeepP06
376 sediments (Figure 7A and C). This lineage is closely related to ANMEs recovered from cold,
377 anoxic habitats, such as seafloor seep sediments, methane hydrates, and hypersaline anoxic
378 basins, and distinct from previously described ANME-1 phylotypes from Sonora Margin cold
379 seep sediments and potentially thermophilic ANME-1 phylotypes from Guaymas Basin
380 hydrothermal sediments (Holler et al., 2011; Biddle et al., 2012). Although ANME-1 archaea
381 were generally assumed to be obligate methanotrophs, this assumption has been challenged
382 and this lineage has been proposed as potentially methanogenic, based on its occurrence and
383 activity in sulfate-depleted sediments (Lloyd et al., 2011; Kevorkian et al., 2020); thus, the
384 biogeochemical role of these archaea would be modulated by the presence or absence of sulfate,
385 or concomitant changes in electron donors. ANME-2 and cultured methanogenic lineages were
386 observed in low percent abundances in all cores in this study (Figure S2). Interestingly, ANME-
387 2 lineages were extremely rare, representing less than 0.05% of any sample and less than 0.02%
388 of any SeepP6 community (Figure S2, Table S3). The prevalence of ANME-1 over ANME-2
389 in the El Puma cores is consistent with the ecophysiological preference of ANME-1 archaea

390 for reducing, sulfidic subsurface sediments, and the preference of ANME-2 for near-surface
391 sediments with intermittently oxidizing conditions (Rossel et al., 2011; Ruff et al., 2015).
392 Previous surveys of mat-covered seep sediments on the Sonora Margin have revealed
393 transitions from ANME-2 towards ANME-1 within short push cores of max. 17 cm depth
394 (Vigneron et al., 2013).

395 Overall, we hypothesize that the Archaeome in the sedimented flanking regions of
396 Guaymas Basin is generally fueled by heterotrophic processes including the degradation of
397 proteins, polymeric carbohydrates (Ziervogel and Arnosti, 2020), and accumulating lipids
398 (Teske et al., 2002) resulting from high sedimentation rates driven by high levels of primary
399 production in the water column. Diverse niche communities allow the Guaymas Archaeome to
400 adapt to environmental challenges, such as hydrothermalism or methane seepage, that are
401 common in the greater Guaymas Basin area; thus, the site-specific complexity of the Guaymas
402 Archaeome underpins its resilience.

403

404 *3. Ecological comparisons: Differentially abundant taxa across sedimentary habitats*

405 *3.1 Near-surface vs. subsurface sediment niches*

406 When comparing the surficial to the subsurface archaeal populations in background control
407 sediments, the majority of OTUs estimated to be differentially abundant are significantly more
408 enriched in the subsurface relative to the surficial sediment, suggesting that benthic archaea
409 prefer subsurface conditions (Figure 8A, B). This trend may also reflect the impact of electron
410 acceptors; for example, oxygen permeates background sediments in Guaymas Basin for at least
411 one centimeter [(Teske et al., 2016), Figure 8B therein]. Following a recently proposed model
412 for benthic microbial communities (Starnawski et al., 2017) the archaeal community at the oxic
413 water-sediment interface likely undergoes downcore selection, based on site-specific selective
414 pressure, resulting in reduced diversity with depth but a higher prevalence of subsurface-
415 adapted taxa within a few thousand years after burial in anoxic subseafloor sediment. Benthic
416 archaea, predominantly Bathyarchaea and MBG-D lineages, survive on residual carbon sources
417 that remain after burial and microbial degradation in surficial sediments (Lloyd et al., 2013).
418 Interestingly, catabolic activity and electron donor diversity, rather than terminal electron
419 acceptor type or burial time, appear to drive bacterial OTU richness in anoxic subseafloor
420 sediment (Walsh et al., 2016). This niche construction mechanism, driven by the biotic
421 microenvironment as opposed to abiotic environmental filtering (Aguilar-Trigueros et al.,
422 2017), is potentially widespread across the large habitable volume represented by non-
423 hydrothermally influenced subseafloor sediments in Guaymas Basin.

424

425 *3.2 OMZ vs. control sediment*

426 When comparing OMZ and surficial background control sedimentary communities, 50% of
427 high abundance OTUs found across both habitats are estimated to be differentially enriched
428 (Figure 8D). Two thirds of the differentially enriched taxa were enriched in the OMZ rather
429 than the surficial background sediments. The MCG lineages MGC-6 and MCG-2 (OTUs 9 and
430 7) and a MBG-D phylotype (OTU 21) are enriched in the surficial background controls relative
431 to the OMZ sediment (Figure 8D). Interestingly, MCG-6 members bear hydrolases that
432 specifically target plant-derived polymeric carbohydrates (Lazar et al., 2016), a potential trait-
433 environment relationship that may differentiate surficial background control from OMZ
434 sediment communities (Figure 8D). When comparing subsurface background control and OMZ
435 sediment communities, the number of OTUs estimated to be differentially enriched was about
436 equal across both environments; however, the majority (68.9%) of high abundance OTUs show
437 no significant differences in their estimated abundances at all (Figure 8E). This implies that the
438 subsurface, rather than surficial, background control communities are more similar to the OMZ
439 communities, a point also corroborated by taxa co-occurrence network analysis (Figure 5B).
440 Thus, oxygen depletion in background subsurface sediment, and oxygen depletion through the
441 overlying oxygen minimum zone of the water column (Calvert, 1964), result in some
442 convergence between archaeal communities across geographically distant and environmentally
443 distinct sedimentary habitats.

444

445 *3.3 Ringvent vs. control sediment*

446 The surficial archaeal communities of Ringvent (RNVP11) and its nearby control site
447 (ContP10) are similar to each other, as indicated by extensive co-occurrence networks (Figure
448 5) and by the lack of differential enrichment between the two cores (Figure 8G). A member of
449 the Hadesarchaea, OTU18, is estimated to be significantly enriched in Ringvent surficial
450 sediment relative to the control; otherwise differences in taxon abundance across these habitats
451 are negligible. Both sites are only 1.6 km apart and therefore most likely share recent
452 depositional histories and microbial inoculum sources, which validates core ContP10 as a site-
453 specific control for assessing the environmental determinants structuring subsurface archaeal
454 communities at Ringvent. The reduction in sequence recovery and, potentially, archaeal
455 community richness in subsurface Ringvent (RNVP11) sediment (Figure 3) is attributed to
456 environmental selection via hydrothermal purging or methane seepage driven by recent sill
457 emplacement that continues to drive hydrothermal circulation, selecting against microbes

458 unable to withstand chemical or thermal changes associated with hydrothermal circulation
459 (Teske et al., 2019). Thus, OTUs may be enriched in Ringvent subsurface sediment relative to
460 its nearby control site (Figure 8H) via two possible ecological scenarios; i) surviving resilient
461 microbes could dominate the habitat after their competitors have been removed, and ii) new
462 arrivals after the disturbance could efficiently recolonize the depopulated surface sediment.

463

464 *3.4 Seep vs. control sediment*

465 Differential abundance comparisons show that the ANME-1, MBG-D, and TMEG lineages are
466 significantly enriched in the seep sediments, compared to controls (Figure 8I-K). Generally,
467 methane seeps are specialized microbial benthic habitats where methanotrophic archaea
468 (ANME) and syntrophic Deltaproteobacteria oxidize methane anaerobically exploiting sulfate
469 as an electron acceptor (Lloyd et al., 2010; Ruff et al., 2015). The dominance of these inter-
470 domain syntrophic partners distinguishes seafloor seep habitats (Ruff et al. 2015). Archaeal
471 community structure in SeepP06 sediments differs little with depth; it is most similar, in terms
472 of taxa overlap, to other samples from the same core (Figures 4 & 5). Therefore, the influence
473 of cold seepage drives community selection to a greater degree than the environmental factors
474 associated with depth-dependent niche differentiation observed in background control
475 sediment.

476 Comparison with other Sonora Margin cores highlights the seep characteristics of core
477 SeepP06. Based on the presence or absence of major archaeal lineages, SeepP06 archaeal
478 communities are similar to surficial (<1mbsf) communities from Sonora Margin cold seeps,
479 predominantly comprised of Thermoplasmata (MBG-D), Bathyarchaea, and ANME lineages
480 (Cruaud et al., 2017). The SeepP06 archaeal communities share dominant archaeal lineages –
481 the Thermoplasmatales (MBG-D), Lokiarchaeota and Bathyarchaeota - with Sonora Margin
482 subsurface sediments [core BCK1, (Vigneron et al., 2014)]. Interestingly, the high proportion
483 of ANME-1 archaea in SeepP06 is not shared by the Sonora Margin subsurface core (Vigneron
484 et al., 2014). The Sonora Margin subsurface sediment core has a deeper methane/sulfate
485 interface than Seep06, ca. 4-5 m instead of 1 m, and contains little sulfide above 5 m depth,
486 indicating strongly attenuated seep influence in core BCK1 compared to SeepP06.

487

488 *4. Core-specific features of the benthic Archaeome*

489 Controls that structure microbial communities in hydrothermal sediments of Guaymas Basin
490 have been studied extensively; for example, extreme temperature and porewater gradients
491 shape microbial population structure, genomic repertoire and activities within a few

492 centimeters depth beneath the seafloor (McKay et al., 2012; McKay et al., 2016; Dombrowski
493 et al., 2018). However, ecological factors influencing microbial life in other sedimentary
494 habitats at Guaymas Basin are comparatively unconstrained. By comparing archaeal
495 communities in diverse sedimentary habitats to background controls representative of standard
496 hemipelagic sedimentation, characteristic responses of the archaeal communities to these
497 distinct environmental settings are becoming apparent. Compaction-induced seepage near the
498 base of the Sonora Margin, and the resulting methane- and sulfide-rich porewater conditions
499 in core SeepP06, selected for anaerobic methane-oxidizing archaea (ANME-1) and MBG-D
500 archaea within the Thermoplasmata, and reduced the relative proportion of Hadesarchaea and
501 Bathyarchaeota. Prior disturbances by hydrothermal impact or strong methane seepage,
502 exemplified in the Ringvent sediments (RNVP11), also strongly differentiated sedimentary
503 archaeal communities from those in background controls. Observed community richness in
504 RNVP11 based on rarefaction curves are reduced throughout much of the core; these results
505 resembled the outcome of a parallel study using different archaeal primers, and bacterial
506 primers as well (Teske et al., 2019). Lastly, anoxic bottom waters impinging on the sediment
507 on the upper Sonora Margin (OMZP12) drive similarities between anoxic surficial sediment at
508 this site and anoxic subsurface background control sediments. The anoxic redox state of the
509 water-sediment interface may also enhance archaeal richness estimates in the upper sediment
510 column, potentially by facilitating the pelagic-benthic transition of archaea, or selecting against
511 a bacteria-dominated interface (Xia et al., 2017). In brief, the archaeal communities of different
512 cores respond in different ways to specific local controls.

513

514 *5. Environmental history determines ecological context*

515 The sediment cores shared similar biogeochemical parameters, such as sedimentary TOC, and
516 organic matter $\delta^{13}\text{C}$, $\delta^{15}\text{N}$ and C:N ratios. Repeatedly, studies of uncultured microbes in the
517 sedimentary subsurface tried to correlate community composition with a wide range of
518 biogeochemical or thermal parameters, in the hope that these linkages provide insights into
519 habitat preference and ecophysiology of uncultured archaea (Durbin and Teske, 2012; Lazar et
520 al., 2015; McKay et al., 2016). While this strategy can yield valuable results, we caution that
521 patterns of archaeal community composition are not deterministically linked to biogeochemical
522 parameters alone, rather, the full context of an ecological interpretation requires that biological
523 and geochemical observations are integrated with the environmental setting and history of a
524 site. For example, the lighter $\delta^{13}\text{C}$ values of sedimentary organic matter in RNVP11 (trending

525 towards -22 ‰ compared to most values clustering between 20 and 21 ‰), the slightly elevated
526 C:N ratios at this site, increased Si concentrations at depth, or the elevated methane content
527 superimposed on seawater-like porewater characteristics, are not in themselves critical factors
528 that determine biological metrics in this core; these factors are significant because they reveal
529 a depositional history of organic-rich sediments overprinted by relatively recent
530 hydrothermalism and methane flux that has left its footprint on the present-day archaeal
531 community. In another example, the archaeal communities of cores SeepP06 and OMZP12
532 would be assumed to be similar, since both sites are rich in sulfide, methane and DIC, and show
533 sulfate depletion concomitant with methane accumulation. However, the distinct
534 environmental settings and histories of these two cores, at the heavily compacted, seep-
535 influenced base of the Sonora Margin (SeepP06), and under the oxygen minimum zone waters
536 of the upper Sonora Margin (OMZP12), ultimately select for different archaeal communities.

537

538 **Conclusion**

539 In the greater Guaymas Basin and Sonora Margin area, complex geological and oceanographic
540 processes impose environmental controls on different sedimentary habitats and their archaeal
541 populations relative to background control sites. In background sediments, archaeal
542 communities vary little with depth after the surface/subsurface transition; here, subsurface
543 communities result primarily from long-term survival likely conferred by relatively reduced
544 mortality (Kirkpatrick et al., 2019). In contrast, localized factors, including water column
545 anoxia, methane seepage, and hydrothermal circulation, constrain the biodiversity and potential
546 biogeochemical activity of sedimentary Archaea across our benthic survey in specific ways.
547 Local sediment biogeochemistry has to be viewed in a broader context – within the history and
548 evolution of a particular site – to reveal its influence on selective survival for certain lineages
549 and subsequent shaping of the resident archaeal ecosystem.

550

551 **Materials and Methods**

552 *Sample Collection.* All samples were collected using piston coring during R/V *El Puma*
553 (Universidad Nacional Autónoma de México, UNAM) Expedition Guaymas14 to the Gulf of
554 California, October 14-27th, 2014. A 5-m long piston core (RNVP11) was obtained on Oct 21,
555 2014 from the central basin within the ring (27°N30.5090/111°W40.6860, 1749 m; core length
556 4.9 m), parallel to a control core (ContP10) approx. 1 mile to the west of Ringvent
557 (27°N30.5193/111°W42.1722; 1731 m depth, 3.93 m core length) collected on the same day.
558 Core SeepP06 was obtained on Oct. 19 from the lower Sonora Margin, near its boundary with

559 the Ridge flanks (27°N38.8367/111°W36.8595; 1681 m depth, 3.95 m core length). Core
560 OMZP12 was taken on Oct. 22 from the upper Sonora Margin (27°N52.1129/111°W41.5902,
561 667 m, 4 m core length) in the oxygen minimum zone as previously determined by water
562 column oxygen profiling (Calvert, 1964). Core ContP03 was collected on Oct. 17 from the
563 northwestern end of the ridge flanks (27°N37.6759/ 111°W52.5740; 1611 m depth, 3.27 m
564 core length. Core ContP13 was obtained on Oct. 22 from the southeastern ridge flank of
565 Guaymas Basin (27°N12.4470/111°W13.7735, 1859m depth, 3.31 m core length).

566

567 *Geochemical Analyses.* Porewater was obtained from freshly collected sediments on RV *El*
568 *Puma* by centrifuging ca. 40 ml sediment samples in 50 ml conical Falcon tubes for ca. 5 to 10
569 minutes, using a Centra CL-2 Tabletop centrifuge (Thermo Scientific) at approx. 1000g, until
570 the sediment had settled and produced ca. 8 to 10 ml of porewater. Porewater was extracted
571 from 5 cm thick sediment samples, which are designated by the top of each sample. For
572 example, a “95 cm” geochemistry sample extends from 95 to 100 cm below the sediment
573 surface. Sulfate, sulfide, methane and DIC porewater profiles for cores SeepP06 to OMZP12
574 were previously published (Teske et al., 2019), and are re-plotted here for comparison with
575 unpublished profiles from cores ContP03 and ContP13. Porewater analyses were performed as
576 previously described, using the colorimetric cline assay for sulfide, ion chromatography for
577 sulfate, and GC-IRMS for DIC and methane (Teske et al., 2019). Carbon and nitrogen isotopic
578 and elemental composition was determined at the Stable Isotope Laboratory (SIL) at the
579 University of California, Santa Cruz (UCSC). Bulk sediment $\delta^{15}\text{N}$ and elemental ratio data
580 were collected using 20mg samples in Sn capsules; organic $\delta^{13}\text{C}$ and elemental
581 composition data were collected using 2.5mg samples of acidified sediment in Sn capsules. All
582 samples were measured by Dumas combustion performed on a Carlo Erba 1108 elemental
583 analyzer coupled to a ThermoFinnigan Delt Plus XP isotope ratio mass spectrometer (EA-
584 IRMS). An in-house gelatin standard, Acetanilide, and an in-house bulk sediment standard,
585 “Monterey Bay Sediment Standard”, were used in all runs. Reproducibility of an in-house
586 matrix-matched sediment standard is $<0.1\text{‰}$ VPDB for $\delta^{13}\text{C}$ and $<0.2\text{‰}$ AIR for $\delta^{15}\text{N}$. Data is
587 corrected for blank, and for drift when appropriate. Carbon and nitrogen elemental composition
588 was estimated based on standards of known composition, for which analytical precision is
589 determined to be better than 1 %. Filtered but unamended porewater samples, stored at 4°C,
590 were used for quantifying multiple stable ions, including silicate, by ion chromatography at
591 GEOMAR, Kiel, Germany (Hensen et al., 2007). All geochemical data in this study are
592 publicly available at the Biological and Chemical Oceanography Data Management Office

593 (BCO-DMO) under the following dataset IDs: 661750, 661658, 66175 and 661808 for
594 Methane, DIC, Sulfate and Sulfide, respectively.

595

596 3. DNA extraction and gene sequencing

597 Samples for DNA sequencing [approx. 2 cm³ each] were obtained by syringe coring at the
598 indicated depth [in cm] below the sediment surface. DNA for all survey sites was extracted
599 from ~0.5-1.0 cm³ sediment sample volumes using the Powersoil DNA extraction kit according
600 to the manufacturer's instructions (QIAGEN, Carlsbad, CA, USA). Archaeal 16S rRNA gene
601 amplicons from DNA extracts were generated using the following primer set: A751F: 5'-CGA
602 CGG TGA GRG RYG AA-3' and A1204R: 5'-TTM GGG GCA TRC NKA CCT-3' (Baker et
603 al., 2003). Amplicons were sequenced on an Illumina MiSeq platform (Illumina, San Diego,
604 CA, USA) at the Center for Biofilm Engineering in Bozeman, Montana. Sequencing run
605 specifications are found in the Visualization and Analysis of Microbial Population Structures
606 (VAMPSs) website (<https://vamps.mbl.edu/resources/primers.php>) (Huse et al., 2014).

607

608 4. Sequence Processing

609 Sequences were processed with *mothur* v.1.39.5 (Schloss et al., 2009) following the *mothur*
610 Illumina MiSeq SOP (Kozich et al., 2013). Briefly, forward and reverse reads were merged
611 into contigs and selected based on primer-specific amplicon length and the following
612 parameters: maximum homopolymers of 6bp, and zero ambiguities. High quality sequences
613 were aligned against the *mothur*-recreated Silva SEED v132 database (Yarza et al., 2010) and
614 subsequently pre-clustered at 1% dissimilarity. As suggested elsewhere (Kozich et al., 2013),
615 spurious sequences are mitigated by abundance ranking and merging with rare sequences based
616 on minimum differences of three base pairs. Chimeras were detected and removed using
617 UCHIME de novo mode (Edgar et al., 2011). Sequences were then clustered, by generating a
618 distance matrix using the average neighbor method, into operational taxonomic units (OTUs,
619 97% similarity cutoff). OTU classification was performed on *mothur* using the SILVA v132
620 database as implemented using the `classify.seqs` command using the Wang algorithm (kmer
621 assignment with 1/8 kmer replacement as bootstrap) and `cutoff=80` (minimal bootstrap value
622 for sequence taxonomy assignment). All sequence data are publically available at the following
623 repository: NCBI under BioProject PRJNA553578 and accession numbers SRX6444849-
624 SRX6444877.

625

626 5. Sequence Analyses

627 5.1 Community Analyses and Visualizations

628 Community analyses were performed in *RStudio* version 0.98.1091 (Racine, 2012),
629 implemented in R version 3.5.2, using the *vegan* (Oksanen et al., 2015) and *phyloseq*
630 (McMurdie and Holmes, 2013) R-packages. Sample richness analyses used the R package
631 *breakaway* (Willis et al. 2017) for inferring precision of diversity estimations given the
632 heterologous sequencing depth. Data were rlog normalized using *DESeq2* (Love et al., 2014)
633 prior to ordination using Bray-Curtis distances. An identical normalization strategy was used
634 on Bray-Curtis distances for co-occurrence network analysis performed using the
635 `makenetwork()` *phyloseq* command and visualized using the *igraph* R-package. *DESeq2* was
636 also used to perform differential abundance analyses of taxa with low abundance taxa ($n < 100$
637 total reads per OTU) removed for the un-rarefied dataset, as suggested elsewhere (McMurdie
638 and Holmes, 2014).

639

640 5.2 Phylogenetic Analyses

641 Sequence alignments were performed using the high speed multiple sequence alignment
642 program MAFFT (Katoh and Standley, 2013) with the command: `mafft --maxiterate 1000 -`
643 `localpair seqs.fasta > aligned.seqs.fasta`. Maximum likelihood trees with 100 bootstrap support
644 were constructed using the RAxML (Stamatakis, 2014) program using the following
645 parameters: `raxmlHPC -f a -m GTRGAMMA -p 12345 -x 12345 -# 100 -s aligned.seqs.fasta -`
646 `n T.tree, -T 4 ML search + bootstrapping`. Newick trees files were uploaded to FigTree v1.4.2
647 for visualization.

648

649 **Data availability.** Geochemical data are available at the BCO-DCO under these reference links:

650 Porewater methane data: <https://www.bco-dmo.org/dataset/661750/data>

651 Porewater sulfate data: <https://www.bco-dmo.org/dataset/661775/data>

652 Porewater DIC data: <https://www.bco-dmo.org/dataset/661658/data>

653 Porewater sulfide: <https://www.bco-dmo.org/dataset/661808/data>

654

655 Acknowledgements

656 Sampling in Guaymas Basin was funded by NSF OCE grant 1449604 “Rapid Proposal:
657 Guaymas Basin site survey cruise for IODP proposal 833” to AT; NSF C-DEBI grant
658 “Characterizing seafloor life and environments in Guaymas Basin” to AT and ACR. This
659 is C-DEBI Publication No. XXX. Thanks go to Zachary Stewart for helping with the

660 sedimentary organic matter geochemistry analyses. We thank the Science crew of R/V *El Puma*
661 for excellent piston coring skills and a very enjoyable cruise.

662

663 **Author Contributions**

664 APT conceived the study. LJM, ACR, and APT collected samples. CM led the *El Puma* cruise
665 and the piston coring effort. AB extracted DNA from sediments. LJM performed sequencing
666 in the lab of MWF. ACR, LJM and CH performed biogeochemical and sedimentological
667 analyses. GAR analyzed the sequence data with phylogeny input from APT. GAR and APT
668 wrote the manuscript with input from all authors.

669

670 **Figure Legends**

671

672 Figure 1: Continental and bathymetric hybrid map depicting the location of Guaymas Basin
673 and Sonora Margin in the Gulf of California, and relevant coring sites of the *El Puma* cruise.
674 The bathymetry blue scale is annotated with 100-meter isobaths; the deepest areas in the axial
675 valley range to just below 2000 meters.

676

677 Figure 2: Geochemical profiles for A) Methane, B) Sulfate, C) Sulfide, and D) DIC porewater
678 concentrations; E) Organic Carbon content in weight %; F) Organic Matter $\delta^{13}\text{C}$ values, and
679 G) $\delta^{15}\text{N}$ values; H) Carbon to Nitrogen ratios, and I) Silica porewater concentrations.
680 Geochemical data for site ContP03 are not available for the analyses depicted in panels E-H.

681

682 Figure 3: Depth mapped rarefaction summaries (color coded to match surveyed sites) for
683 complete high quality sequence dataset depicting richness as number of OTUs (97% similarity
684 clustered) observed per sequences sampled. A) samples near the interface (0-10cmbsf), B)
685 samples from ~100cmbsf, C) samples from ~200cmbsf, D) samples from ~300cmbsf, E)
686 samples from depths greater than or approximately equal 400cmbsf.

687

688 Figure 4: A) Two-dimensional Principal Coordinate Analyses of Bray-Curtis dissimilarity
689 distances from r-log normalized sequence count data. Each community plotted is color-coded
690 to the core site and numerical labels indicate sediment depth (cmbsf). The first and second axes
691 explain 29.8 and 14.8% of the variance, respectively. Environmental metadata superimposed
692 on ordination plot are B) methane, C) sulfate, D) sulfide, and E) DIC concentrations, F) water
693 depth, and G) sediment depth.

694

695 Figure 5. Network analysis based on the co-occurrence of all OTUs at in each sample. Nodes
696 represent all archaeal communities analyzed in this study. Nodes are color-coded to match
697 descriptions from Figure 1A. Edges are unweighted interactions depicting OTU co-occurrence
698 meeting arbitrary thresholds. A) Co-occurrence network threshold set at a maximum Bray-
699 Curtis distance of 0.8. B) Co-occurrence network threshold set at a maximum Bray-Curtis
700 distance of 0.5.

701

702 Figure 6: Class-level community composition of all depths for all cores in this study. Core
703 labels are color-coded to match the collection sites depicted in the bathymetric map in Figure
704 1.

705

706 Figure 7: A) Heatmap depicting percent abundance distribution for the 25 most abundant
707 OTUs, representing 73.0% of all high-quality sequences in this study, for all cores and across
708 all depths. Core labels are color-coded to match the collection sites depicted in the bathymetric
709 map in Figure 1A. The phylogenetic association of each OTU lineage is depicted above each
710 OTU header. The percent of total reads represented by the 25 most abundant OTUs in each
711 community is shown in the column labeled “% of community”. Maximum likelihood
712 phylogenetic trees, with 100 bootstrap support, placing the top 25 most abundant OTUs within
713 the following lineages: B) Bathyarchaea, C) the Euryarchaeotal lineages MBG-D, TMEG,
714 SAGMEG, and ANMEs.

715

716 Figure 8: Differential Abundance Analyses bases on Wald’s test (significance: $\alpha = 0.01$).
717 A) Ordination depicting archaeal community clustering for surface and subsurface samples of
718 control sites ContP3, ContP10, and ContP13. B) Differentially abundant OTUs in near-surface
719 versus subsurface communities from control sites. C) Ordination depicting community
720 clustering in OMZP12, and surficial vs. subseafloor control sites. D) Differentially abundant
721 OTUs in OMZP12 compared to surficial and E) subsurface communities from control sites. F)
722 Ordination depicting community clustering in RNVP11 to Cont10. Differentially abundant
723 OTUs in RNVP11 and Cont10 for G) surface samples and H) subsurface samples. I) Ordination
724 depicting community clustering in SeepP06, and surficial and subseafloor control sites.
725 Differentially abundant OTUs in SeepP06 samples compared to J) surficial and K) subsurface
726 communities from control sites. Note: OTUs 13, 17 and 21 are color-coded as “unclassified”

727 by SILVA132, but the phylogeny identifies them as members of MCG-13 (OTUs 13 and 17)
728 and MBG-D (OTU 21).

729

730 **Works cited:**

731

732 Aguilar-Trigueros, C.A., Rillig, M.C., and Ballhausen, M.-B. (2017). Environmental filtering
733 is a relic. A response to Cadotte and Tucker. *Trends in Ecol. & Evol.* 32, 882-884. doi:
734 10.1016/j.tree.2017.09.013.

735 Baker, B.J., Saw, J.H., Lind, A.E., Lazar, C.S., Hinrichs, K.U., Teske, A.P., and Ettema, T.J.
736 (2016). Genomic inference of the metabolism of cosmopolitan subsurface Archaea,
737 Hadesarchaea. *Nat. Microbiol.* 1, 16002. doi: 10.1038/nmicrobiol.2016.2.

738 Baker, G.C., Smith, J.J., and Cowan, D.A. (2003). Review and re-analysis of domain-specific
739 16S primers. *J. of Microbiol. Meth.* 55, 541-555. doi: 10.1016/j.mimet.2003.08.009.

740 Biddle, J.F., Cardman, Z., Mendlovitz, H., Albert, D.B., Lloyd, K.G., Boetius, A., and Teske,
741 A. (2012). Anaerobic oxidation of methane at different temperature regimes in
742 Guaymas Basin hydrothermal sediments. *ISME J.* 6, 1018-1031. doi:
743 10.1038/ismej.2011.164.

744 Calvert, S.E. (1964). "Factors affecting distribution of laminated diatomaceous sediments in
745 the Gulf of California" In Marine Geology of the Gulf of California, Vol. 3, eds. T.H.
746 van Andel and G.G. Shor, (Tulsa: American Association of Petroleum Geologists
747 *Memoir*) 3, 311-330.

748 Calvert, S.E. (1966). Origin of diatom-rich, varved sediments from the Gulf of California. *J.*
749 *Geology* 74, 546-565. doi: <https://www.jstor.org/stable/30059298>.

750 Campbell, A.C., and Gieskes, J.M. (1984). Water column anomalies associated with
751 hydrothermal activity in the Guaymas Basin, Gulf of California. *Earth and Planet. Sci.*
752 *Lett.* 68, 57-72.

753 Cruaud, P., Vigneron, A., Pignet, P., Caprais, J.-C., Lesongeur, F., Toffin, L., Godfroy, A., and
754 Cambon-Bonavita, M.-A. (2017). Comparative study of guaymas basin microbiomes:
755 cold seeps vs. hydrothermal vents sediments. *Front. Mar. Sci.* 4. doi:
756 10.3389/fmars.2017.00417.

757 Didyk, B.M., and Simoneit, B.R.T. (1989). Hydrothermal oil of Guaymas Basin and
758 implications for petroleum formation mechanisms. *Nature* 342, 65-69.

759 Dombrowski, N., Teske, A., and Baker, B.J. (2018). Expansive microbial metabolic diversity
760 and biodiversity in dynamic Guaymas Basin hydrothermal sediments. *Nature Comm.*
761 9. doi: <https://doi.org/10.1038/s41467-018-07418-0>.

762 Durbin, A.M., and Teske, A. (2012). Archaea in organic-lean and organic-rich marine
763 subsurface sediments: an environmental gradient reflected in distinct phylogenetic
764 lineages. *Front. Microbiol.* 3, 168. doi: 10.3389/fmicb.2012.00168.

765 Edgar, R.C., Haas, B.J., Clemente, J.C., Quince, C., and Knight, R. (2011). UCHIME improves
766 sensitivity and speed of chimera detection. *Bioinformatics* 27, 2194-2200. doi:
767 10.1093/bioinformatics/btr381.

768 Evans, P., Parks, D.H., Chadwick, G.L., Robbins, S.J., Orphan, V.J., Golding, S.D., and Tyson,
769 G.W. (2015). Methane metabolism in the archaeal phylum Bathyarchaeota revealed by
770 genome-centric metagenomics. *Science* 350.

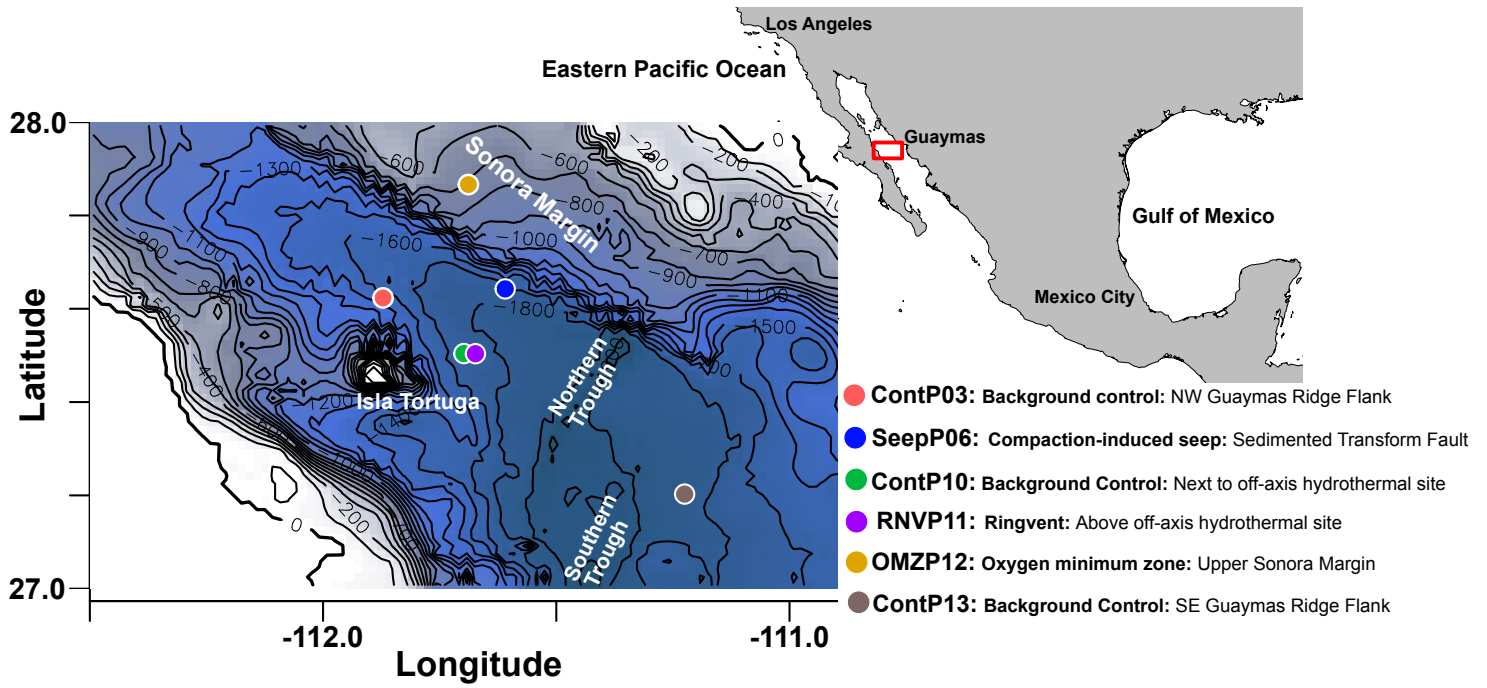
771 Geilert, S., Hensen, C., Schmidt, M., Liebetrau, V., Scholz, F., Doll, M., Deng, L., Fiskal, A.,
772 Lever, M.A., Su, C.-C., Schloemer, S., Sarkar, S., Thiel, V., and Berndt, C. (2018). On
773 the formation of hydrothermal vents and cold seeps in the Guaymas Basin, Gulf of
774 California. *Biogeosciences* 15, 5715-5731. doi: 10.5194/bg-15-5715-2018.

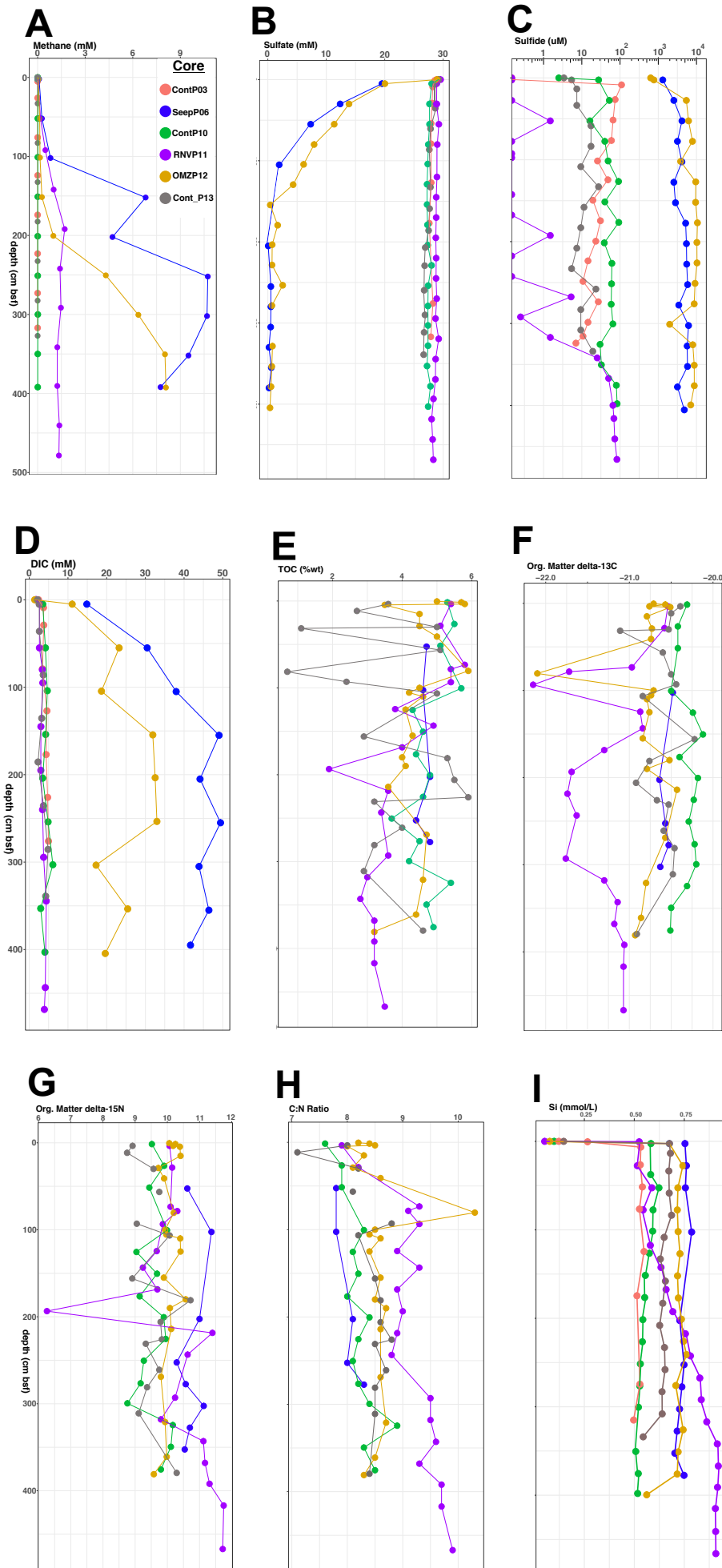
- 775 He, Y., Li, M., Perumal, V., Feng, X., Fang, J., Xie, J., Sievert, S.M., and Wang, F. (2016).
776 Genomic and enzymatic evidence for acetogenesis among multiple lineages of the
777 archaeal phylum Bathyarchaeota widespread in marine sediments. *Nat Microbiol* 1,
778 16035. doi: 10.1038/nmicrobiol.2016.35.
- 779 Hensen, C., Nuzzo, M., Hornibrook, E., Pinheiro, L.M., Bock, B., Magalhães, V.H., and
780 Brückmann, W. (2007). Sources of mud volcano fluids in the Gulf of Cadiz—
781 indications for hydrothermal imprint. *Geochim. et Cosmochim. Acta* 71, 1232-1248.
782 doi: 10.1016/j.gca.2006.11.022.
- 783 Holler, T., Widdel, F., Knittel, K., Amann, R., Kellermann, M.Y., Hinrichs, K.U., Teske, A.,
784 Boetius, A., and Wegener, G. (2011). Thermophilic anaerobic oxidation of methane by
785 marine microbial consortia. *ISME J.* 5, 1946-1956. doi: 10.1038/ismej.2011.77.
- 786 Huse, S.M., Mark Welch, D., Voorhis, A., Shipunova, A., Morrison, H.G., Eren, A.M., and
787 Sogin, M. (2014). VAMPS: a website for visualization and analysis of microbial
788 population structures. *BMC Bioinformatics* 15. doi: 10.1186/1471-2105-15-41.
- 789 Katoh, K., and Standley, D.M. (2013). MAFFT multiple sequence alignment software version
790 7: improvements in performance and usability. *Mol. Biol. Evol.* 30, 772-780. doi:
791 10.1093/molbev/mst010.
- 792 Kevorkian, R., Callahan, S., Winstead, R., and Lloyd, K.G. (2020). ANME-1 archaea drive
793 methane accumulation and removal in estuarine sediment. *bioRxiv* 2020.02.24.963215.
794 doi: 10.1101/2020.02.24.963215.
- 795 Kirkpatrick, J.B., Walsh, E.A., and D'Hondt, S. (2019). Microbial Selection and Survival in
796 Subseafloor Sediment. *Front. Microbiol.* 10. doi: 10.3389/fmicb.2019.00956.
- 797 Kozich, J.J., Westcott, S.L., Baxter, N.T., Highlander, S.K., and Schloss, P.D. (2013).
798 Development of a dual-index sequencing strategy and curation pipeline for analyzing
799 amplicon sequence data on the MiSeq Illumina sequencing platform. *Appl. Environ.*
800 *Microbiol.* 79, 5112-5120.
- 801 Kubo, K., Lloyd, K.G., J.F., B., Amann, R., Teske, A., and Knittel, K. (2012). Archaea of the
802 Miscellaneous Crenarchaeotal Group are abundant, diverse and widespread in marine
803 sediments. *ISME J.* 6, 1949-1965. doi: 10.1038/ismej.2012.37.
- 804 Lazar, C.S., Baker, B.J., Seitz, K., Hyde, A.S., Dick, G.J., Hinrichs, K.U., and Teske, A.P.
805 (2016). Genomic evidence for distinct carbon substrate preferences and ecological
806 niches of Bathyarchaeota in estuarine sediments. *Environ. Microbiol.* 18, 1200-1211.
807 doi: 10.1111/1462-2920.13142.
- 808 Lazar, C.S., Biddle, J.F., Meador, T.B., Blair, N., Hinrichs, K.U., and Teske, A.P. (2015).
809 Environmental controls on intragroup diversity of the uncultured benthic archaea of the
810 miscellaneous Crenarchaeotal group lineage naturally enriched in anoxic sediments of
811 the White Oak River estuary (North Carolina, USA). *Environ. Microbiol.* 17, 2228-
812 2238. doi: 10.1111/1462-2920.12659.
- 813 Lever, M.A., Heuer, V.B., Morono, Y., Masui, N., Schmidt, F., Alperin, M.J., Inagaki, F.,
814 Hinrichs, K.-U., and Teske, A. (2010). Acetogenesis in deep subseafloor sediments of
815 the Juan de Fuca Ridge Flank: A synthesis of geochemical, thermodynamic, and gene-
816 based evidence. *Geomicrobiol. J.* 27, 183-211. doi: 10.1080/01490450903456681.
- 817 Lizarralde, D., Axen, G.J., Brown, H.E., Fletcher, J.M., Gonzalez-Fernandez, A., Harding,
818 A.J., Holbrook, W.S., Kent, G.M., Paramo, P., Sutherland, F., and Umhoefer, P.J.
819 (2007). Variation in styles of rifting in the Gulf of California. *Nature* 448, 466-469.
820 doi: 10.1038/nature06035.
- 821 Lizarralde, D., Soule, S.A., Seewald, J.S., and Proskurowski, G. (2010). Carbon release by off-
822 axis magmatism in a young sedimented spreading centre. *Nat. Geosci.* 4, 50-54. doi:
823 10.1038/ngeo1006.

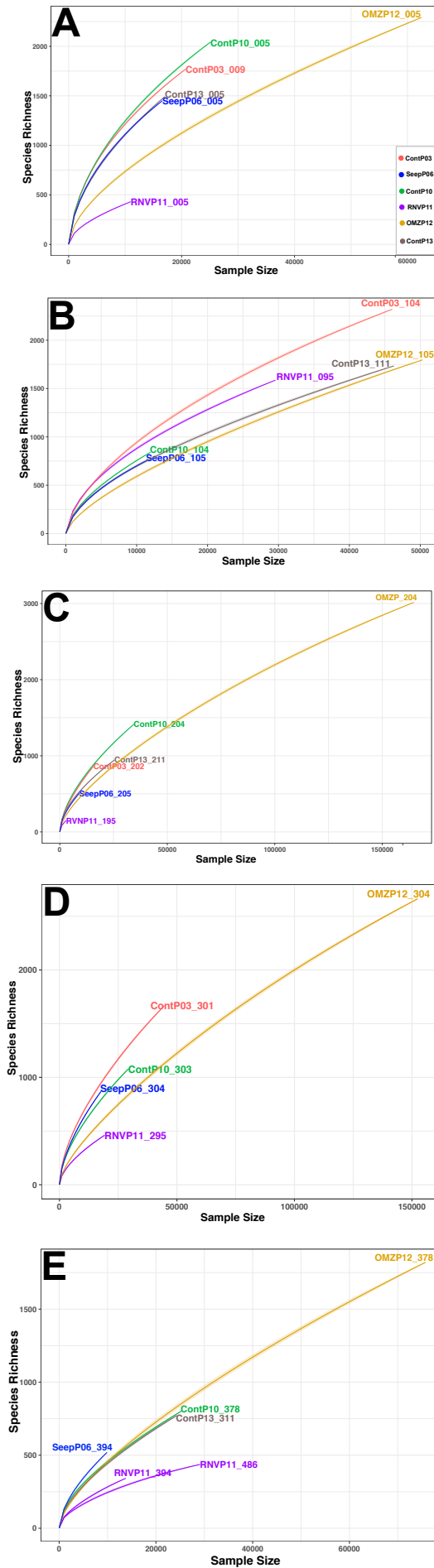
- 824 Lloyd, K.G., Albert, D.B., Biddle, J.F., Chanton, J.P., Pizarro, O., and Teske, A. (2010). Spatial
825 structure and activity of sedimentary microbial communities underlying a *Beggiatoa*
826 spp. mat in a Gulf of Mexico hydrocarbon seep. *PLoS One* 5, e8738. doi:
827 10.1371/journal.pone.0008738.
- 828 Lloyd, K.G., Alperin, M.J., and Teske, A. (2011). Environmental evidence for net methane
829 production and oxidation in putative ANaerobic MEthanotrophic (ANME) archaea.
830 *Environ. Microbiol.* 13, 2548-2564. doi: 10.1111/j.1462-2920.2011.02526.x.
- 831 Lloyd, K.G., Schreiber, L., Petersen, D.G., Kjeldsen, K.U., Lever, M.A., Steen, A.D.,
832 Stepanauskas, R., Richter, M., Kleindienst, S., Lenk, S., Schramm, A., and Jorgensen,
833 B.B. (2013). Predominant archaea in marine sediments degrade detrital proteins.
834 *Nature* 496, 215-218. doi: 10.1038/nature12033.
- 835 Lonsdale, P., and Becker, K. (1985). Hydrothermal plumes, hot springs, and conductive heat
836 flow in the Southern Trough of Guaymas Basin. *Earth and Planet. Sci. Lett.* 73, 211-
837 225.
- 838 Love, M.I., Huber, W., and Anders, S. (2014). Moderated estimation of fold change and
839 dispersion for RNA-seq data with DESeq2. *Genome Biol.* 15, 550. doi:
840 10.1186/s13059-014-0550-8.
- 841 Martens, C.S. (1990). Generation of short chain organic acid anions in hydrothermally altered
842 sediments of the Guaymas Basin, Gulf of California. *Appl. Geochem.* 5, 71-76.
- 843 McKay, L., Klokman, V.W., Mendlovitz, H.P., Larowe, D.E., Hoer, D.R., Albert, D., Amend,
844 J.P., and Teske, A. (2016). Thermal and geochemical influences on microbial
845 biogeography in the hydrothermal sediments of Guaymas Basin, Gulf of California.
846 *Environ Microbiol Rep* 8, 150-161. doi: 10.1111/1758-2229.12365.
- 847 McKay, L.J., MacGregor, B.J., Biddle, J.F., Albert, D.B., Mendlovitz, H.P., Hoer, D.R., Lipp,
848 J.S., Lloyd, K.G., and Teske, A.P. (2012). Spatial heterogeneity and underlying
849 geochemistry of phylogenetically diverse orange and white *Beggiatoa* mats in Guaymas
850 Basin hydrothermal sediments. *Deep Sea Res. I* 67, 21-31. doi:
851 10.1016/j.dsr.2012.04.011.
- 852 McMurdie, P.J., and Holmes, S. (2013). phyloseq: an R package for reproducible interactive
853 analysis and graphics of microbiome census data. *PLoS One* 8, e61217. doi:
854 10.1371/journal.pone.0061217.
- 855 McMurdie, P.J., and Holmes, S. (2014). Waste not, want not: why rarefying microbiome data
856 is inadmissible. *PLoS Comput. Biol.* 10. doi: 10.1371/.
- 857 Oksanen, J., Blanchet, F.G., Kindt, R., Legendre, P., Minchin, P.R., O'hara, R.B., Simpson,
858 G.L., Solymos, P., Stevens, M.H.H., and Wagner, H. (2015). vegan: Community
859 Ecology Package. R Package Version 2.2-1. Available online at: [http://cran.r-](http://cran.r-project.org/package=vegan)
860 [project.org/package=vegan](http://cran.r-project.org/package=vegan).
- 861 Paull, C.K., Ussler, W., Peltzer, E.T., Brewer, P.G., Keaten, R., Mitts, P.J., Nealon, J.W.,
862 Greinert, J., Herguera, J.-C., and Elena Perez, M. (2007). Authigenic carbon entombed
863 in methane-soaked sediments from the northeastern transform margin of the Guaymas
864 Basin, Gulf of California. *Deep Sea Res. II* 54, 1240-1267. doi:
865 10.1016/j.dsr2.2007.04.009.
- 866 Peter, J.M., and Scott, S.D. (1988). Mineralogy, composition, and fluid-inclusion
867 microthermometry of seafloor hydrothermal deposits in the southern trough of
868 Guaymas Basin, Gulf of California. *Canadian Mineralogist* 26, 567-587.
- 869 Portail, M., Olu, K., Escobar-Briones, E., Caprais, J.C., Menot, L., Waeles, M., Cruaud, P.,
870 Sarradin, P.M., Godfroy, A., and Sarrazin, J. (2015). Comparative study of vent and
871 seep macrofaunal communities in the Guaymas Basin. *Biogeosciences* 12, 5455-5479.
872 doi: 10.5194/bg-12-5455-2015.

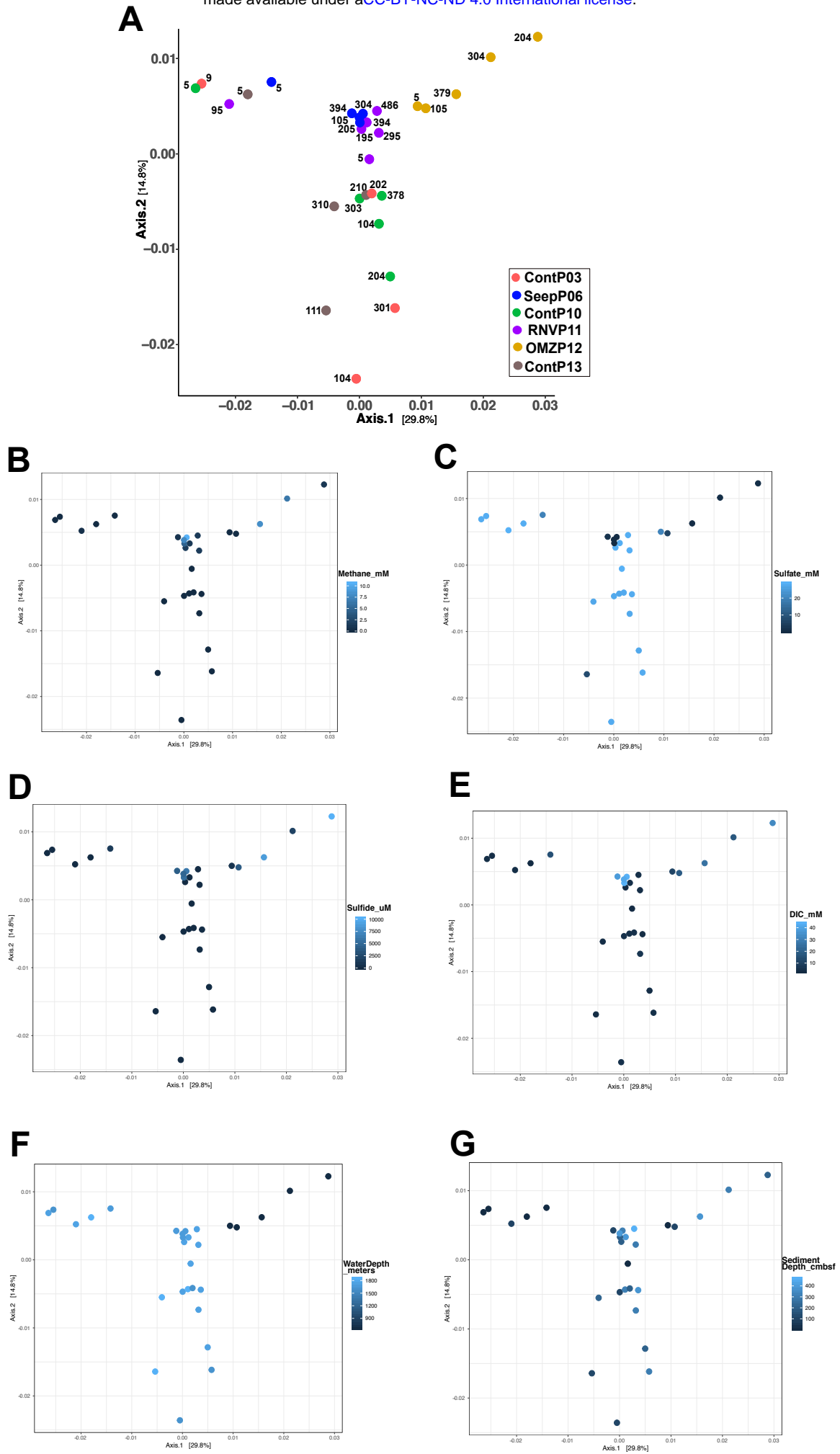
- 873 Racine, J.S. (2012). RStudio: A Platform-Independent IDE for R and Sweave. *Journal of*
874 *Applied Econometrics* 27, 167-172. doi: 10.1002/jae.1278.
- 875 Rossel, P.E., Elvert, M., Ramette, A., Boetius, A., and Hinrichs, K.-U. (2011). Factors
876 controlling the distribution of anaerobic methanotrophic communities in marine
877 environments: Evidence from intact polar membrane lipids. *Geochim. Cosmochim.*
878 *Acta* 75, 164-184. doi: 10.1016/j.gca.2010.09.031.
- 879 Ruff, S.E., Biddle, J.F., Teske, A.P., Knittel, K., Boetius, A., and Ramette, A. (2015). Global
880 dispersion and local diversification of the methane seep microbiome. *Proc. Natl. Acad.*
881 *Sci. U. S. A.* 112, 4015-4020. doi: 10.1073/pnas.1421865112.
- 882 Schloss, P.D., Westcott, S.L., Ryabin, T., Hall, J.R., Hartmann, M., Hollister, E.B., Lesniewski,
883 R.A., Oakley, B.B., Parks, D.H., Robinson, C.J., Sahl, J.W., Stres, B., Thallinger, G.G.,
884 Van Horn, D.J., and Weber, C.F. (2009). Introducing mothur: open-source, platform-
885 independent, community-supported software for describing and comparing microbial
886 communities. *Appl. Environ. Microbiol.* 75, 7537-7541. doi: 10.1128/AEM.01541-09.
- 887 Seewald, J.S., Seyfried, W.E., and Thornton, E.C. (1990). Organic-rich sediment alteration: an
888 experimental and theoretical study at elevated temperatures and pressures. *Appl.*
889 *Geochem.* 5, 193-209.
- 890 Simoneit, B.R.T., Lonsdale, P., Edmond, J.M., and Shank Iii, W.C. (1990). Deep-water
891 hydrocarbon seeps in Guaymas Basin, Gulf of California *Appl. Geochem.* 5, 41-49.
- 892 Spang, A., Caceres, E.F., and Ettema, T.J.G. (2017). Genomic exploration of the diversity,
893 ecology, and evolution of the archaeal domain of life. *Science* 357. doi:
894 10.1126/science.aaf3883.
- 895 Stamatakis, A. (2014). RAxML version 8: a tool for phylogenetic analysis and post-analysis of
896 large phylogenies. *Bioinformatics* 30, 1312-1313. doi: 10.1093/bioinformatics/btu033.
- 897 Starnawski, P., Bataillon, T., Ettema, T.J., Jochum, L.M., Schreiber, L., Chen, X., Lever, M.A.,
898 Polz, M.F., Jorgensen, B.B., Schramm, A., and Kjeldsen, K.U. (2017). Microbial
899 community assembly and evolution in seafloor sediment. *Proc. Natl. Acad. Sci. U.*
900 *S. A.* 114, 2940-2945. doi: 10.1073/pnas.1614190114.
- 901 Teske, A., De Beer, D., McKay, L.J., Tivey, M.K., Biddle, J.F., Hoer, D., Lloyd, K.G., Lever,
902 M.A., Roy, H., Albert, D.B., Mendlovitz, H.P., and Macgregor, B.J. (2016). The
903 Guaymas Basin Hiking Guide to Hydrothermal Mounds, Chimneys, and Microbial
904 Mats: Complex Seafloor Expressions of Subsurface Hydrothermal Circulation. *Front.*
905 *Microbiol.* 7, 75. doi: 10.3389/fmicb.2016.00075.
- 906 Teske, A., Hinrichs, K.U., Edgcomb, V., De Vera Gomez, A., Kysela, D., Sylva, S.P., Sogin,
907 M.L., and Jannasch, H.W. (2002). Microbial Diversity of Hydrothermal Sediments in
908 the Guaymas Basin: Evidence for Anaerobic Methanotrophic Communities. *Appl.*
909 *Environ. Microbiol.* 68, 1994-2007. doi: 10.1128/aem.68.4.1994-2007.2002.
- 910 Teske, A., McKay, L., Ravelo, A.C., Aiello, I., Mortera, C., Núñez-Useche, F., Canet, C.,
911 Chanton, J.P., Brunner, B., Hensen, C., Ramírez, G.A., Sibert, R.J., Turner, T., White,
912 D., Chambers, C.R., Buckley, A., Joye, S.B., Soule, S.A., and Lizarralde, D. (2019).
913 Characteristics and evolution of sill-driven off-axis hydrothermalism in Guaymas
914 Basin- the Ringvent site. *Scientific Reports* 9. doi: 10.1038/s41598-019-50200-5.
- 915 Vigneron, A., Cruaud, P., Pignet, P., Caprais, J.C., Cambon-Bonavita, M.A., Godfroy, A., and
916 Toffin, L. (2013). Archaeal and anaerobic methane oxidizer communities in the Sonora
917 Margin cold seeps, Guaymas Basin (Gulf of California). *ISME J.* 7, 1595-1608. doi:
918 10.1038/ismej.2013.18.
- 919 Vigneron, A., Cruaud, P., Roussel, E.G., Pignet, P., Caprais, J.C., Callac, N., Ciobanu, M.C.,
920 Godfroy, A., Cragg, B.A., Parkes, J.R., Van Nostrand, J.D., He, Z., Zhou, J., and Toffin,
921 L. (2014). Phylogenetic and functional diversity of microbial communities associated

- 922 with subsurface sediments of the Sonora Margin, Guaymas Basin. *PLoS One* 9,
923 e104427. doi: 10.1371/journal.pone.0104427.
- 924 Von Damm, K.L., Edmond, J.M., Measures, C.I., and Grant, B. (1985). Chemistry of
925 submarine hydrothermal solutions at Guaymas Basin, Gulf of California. *Geochim.*
926 *Cosmochim. Acta* 49, 2221-2237.
- 927 Walsh, E.A., Kirkpatrick, J.B., Pockalny, R., Sauvage, J., Spivack, A.J., Murray, R.W., Sogin,
928 M.L., and D'Hondt, S. (2016). Relationship of bacterial richness to organic degradation
929 rate and sediment age in seafloor sediment. *Appl. Environ. Microbiol.* 82, 4994-
930 4999. doi: 10.1128/AEM.00809-16.
- 931 Welhan, J.A., and Lupton, J.E. (1987). Light Hydrocarbon Gases in Guaymas Basin
932 Hydrothermal Fluids: Thermogenic Versus Abiogenic Origin. *AAPG Bulletin* 71. doi:
933 10.1306/94886d76-1704-11d7-8645000102c1865d.
- 934 Willis, A., and Bunge, J. (2015). Estimating diversity via frequency ratios. *Biometrics* 71,
935 1042-1049. doi: 10.1111/biom.12332.
- 936 Xia, X., Guo, W., and Liu, H. (2017). Basin Scale Variation on the Composition and Diversity
937 of Archaea in the Pacific Ocean. *Front. Microbiol.* 8, 2057. doi:
938 10.3389/fmicb.2017.02057.
- 939 Yarza, P., Ludwig, W., Euzéby, J., Amann, R., Schleifer, K.H., Glöckner, F.O., and Rossello-
940 Mora, R. (2010). Update of the All-Species Living Tree Project based on 16S and 23S
941 rRNA sequence analyses. *Syst. Appl. Microbiol.* 33, 291-299. doi:
942 10.1016/j.syapm.2010.08.001.
- 943 Yu, T., Wu, W., Liang, W., Lever, M.A., Hinrichs, K.U., and Wang, F. (2018). Growth of
944 sedimentary Bathyarchaeota on lignin as an energy source. *Proc Natl Acad Sci U S A*
945 115, 6022-6027. doi: 10.1073/pnas.1718854115.
- 946 Zhou, Z., Liu, Y., Lloyd, K.G., Pan, J., Yang, Y., Gu, J.D., and Li, M. (2019). Genomic and
947 transcriptomic insights into the ecology and metabolism of benthic archaeal
948 cosmopolitan, Thermopfundales (MBG-D archaea). *ISME J.* 13, 885-901. doi:
949 10.1038/s41396-018-0321-8.
- 950 Ziervogel, K., and Arnosti, C. (2020). Substantial Carbohydrate Hydrolase Activities in the
951 Water Column of the Guaymas Basin (Gulf of California). *Front. Mar. Sci.* 6. doi:
952 10.3389/fmars.2019.00815.
- 953

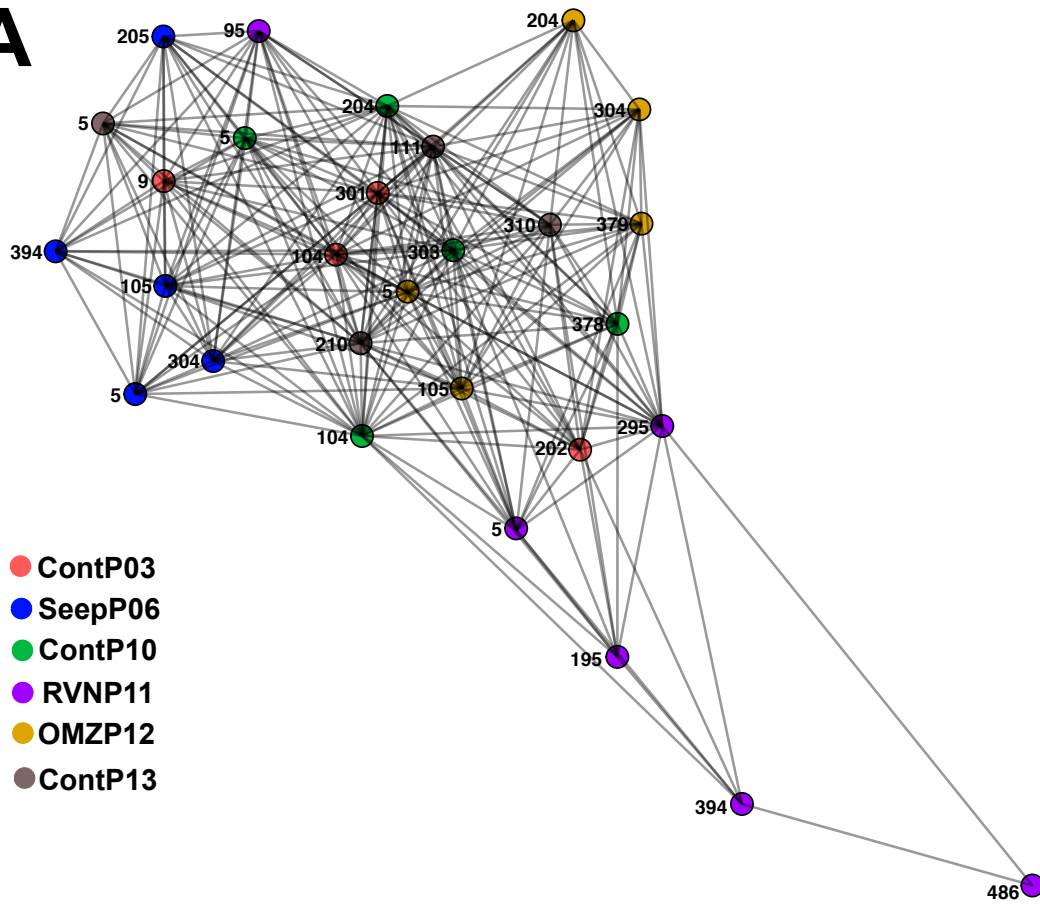








A



B

